AGU PUBLICATIONS

JGR

Journal of Geophysical Research: Atmospheres

RESEARCH ARTICLE
10.1002/2015JD024136

Key Points:
- Downward transport of NO_x through the mesopause is explored
- Molecular diffusion and advection are the main drivers
- Direction and strength of advection vary strongly on the time scale of a few days during the SSW

Correspondence to:
K. Meraner,
katharina.meraner@mpimet.mpg.de

Citation:
Meraner, K., and H. Schmidt (2016), Transport of nitrogen oxides through the winter mesopause in HAMMONIA, *J. Geophys. Res. Atmos.*, *121*, 2556–2570, doi:10.1002/2015JD024136.

Received 27 AUG 2015
Accepted 23 FEB 2016
Accepted article online 27 FEB 2016
Published online 18 MAR 2016

Transport of nitrogen oxides through the winter mesopause in HAMMONIA

Katharina Meraner[1] and Hauke Schmidt[1]

[1] Max Planck Institute for Meteorology, Hamburg, Germany

Abstract We analyze the importance of individual transport processes for the winter polar downward transport of nitrogen oxides (NO_x) from the thermosphere to the mesosphere. The downward transport of NO_x produced by energetic particle precipitation induces chemical alterations in the middle atmosphere and influences ozone chemistry. However, it remains unclear how much each transport process contributes to the downward transport. We use simulations of the atmospheric general circulation and chemistry model HAMMONIA (Hamburg Model of Neutral and Ionized Atmosphere) for the extended winter 2008/2009 with a passive tracer. The model enables us to separate the contributions of advection, eddy and molecular diffusion on the total transport by switching off processes. The results show that molecular diffusion and resolved vertical mixing due to advection effectively transport NO_x to the mesosphere. While the impact of molecular diffusion on the transport rapidly decreases below 0.001 hPa, the impact of advection increases. Around the central date of the sudden stratospheric warming in January 2009, advection is strongly enhanced in the thermosphere and mesosphere and the downward transport through the mesopause region is almost entirely driven by advection. Eddy diffusion has limited impact on the transport in the upper mesosphere and negligible impact on the transport in the thermosphere. If eddy diffusion is enhanced as suggested by observations, it can potentially have a larger impact on transport through the mesopause than was previously assumed.

1. Introduction

Energetic particle precipitation (EPP) induces large chemical disturbances, mainly in the polar winter middle and upper atmosphere. *Seppälä and Clilverd* [2014] showed that the impact from EPP events on the northern hemispheric stratosphere may be of the same magnitude as the impact from variability in solar UV irradiance.

Already in the 1970s and 1980s, it was discovered that EPP is a major source for nitrogen oxides ($NO_x = N + NO + NO_2$) and odd hydrogen ($HO_x = H + OH + HO_2$) [*Crutzen et al.*, 1975; *Solomon et al.*, 1981; *Rusch et al.*, 1981]. Both chemical components catalytically deplete ozone in the middle atmosphere, NO_x mainly below and HO_x above about 45 km. However, HO_x is short lived in the middle atmosphere and the impact of an EPP event on the HO_x budget is of short duration. In contrast, NO_x can persist up to several months in the polar-night stratosphere. Outside the polar night, NO_x is quickly destroyed by photodissociation, while inside the winter polar vortex, NO_x is transported downward from its original location in the polar upper mesosphere and lower thermosphere to the polar stratosphere [*Funke et al.*, 2007; *Sinnhuber et al.*, 2014]. There NO_x contributes to ozone destruction. The effect of the downward transport of NO_x is called the indirect EPP effect, while the effect of the local production of NO_x and HO_x in the polar stratosphere and mesosphere is called the direct EPP effect [*Randall et al.*, 2006, 2007].

Several observational studies have given evidence for the indirect EPP effect [e.g., *Funke et al.*, 2005; *Semeniuk et al.*, 2005]. The downward transport of NO_x even exceeds the direct EPP impact of the large solar proton event in October and November 2003 on the NO_x budget above 60 km [*Sinnhuber et al.*, 2014]. However, it remains unclear which transport processes are responsible for the descent of NO_x from the thermosphere to the mesosphere.

In this study, we analyze the importance of individual transport processes for the winter polar downward transport of NO_x from the thermosphere to the stratosphere using the extended winter 2008/2009 as an example. We use simulations of the general circulation and chemistry model HAMMONIA (Hamburg Model of Neutral and Ionized Atmosphere). Our results clarify which dynamical conditions favor the intrusion of

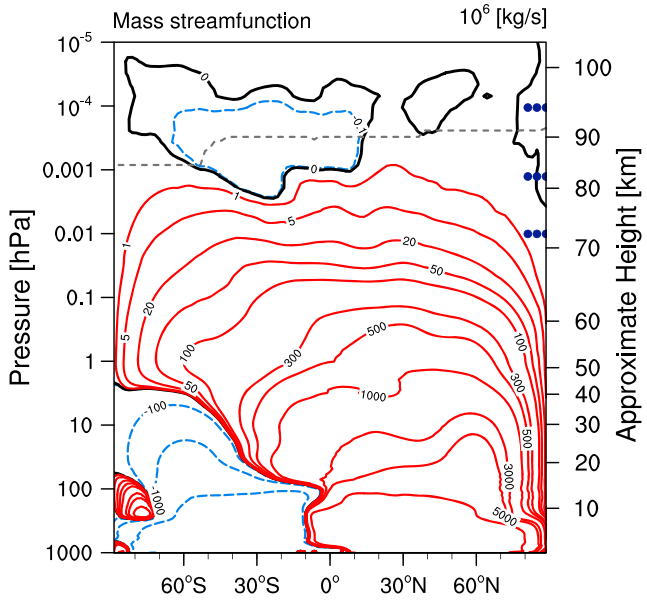

Figure 1. Zonal mean residual stream function for November and December 2008 calculated by HAMMONIA. Red positive values correspond to a clockwise circulation and blue negative values to a counterclockwise circulation. The gray dashed line above 0.001 hPa represents the height of the mesopause. The location and height of three emission areas used on the numerical experiments of this study are marked with blue dots.

thermospheric air to the mesosphere and indicate how potential trends in eddy diffusion, as discussed by *Hoffmann et al.* [2011] and *Emmert et al.* [2012], may change the transport characteristics.

At the winter polar mesospheric to the stratospheric altitudes, the downward transport is dominated by the residual circulation, which has an ascending branch over the summer pole and a descending branch over the winter pole [*Brasseur and Solomon*, 2005]. Hence, at these altitudes it has been shown that NO_x is dominantly transported by advection [*Smith et al.*, 2011]. The dominance of advection below the mesopause is highlighted in Figure 1 by the mass stream function, which describes the net trajectory of air parcels and is calculated using 6-hourly values of the Transformed Eulerian Mean (TEM) circulation. NO_x is frequently produced by EPP in the polar lower thermosphere, but the mass stream function in Figure 1 shows no clear advective downward transport from the thermosphere to the mesosphere. Hence, this downward transport remains an open question, which we will tackle in this study. The only way to transport a tracer across the streamlines is either due to photochemical processes or due to eddy or molecular diffusion. We do not consider photochemical processes and concentrate on the transport.

The total transport can be split into three processes: advection, eddy diffusion, and molecular diffusion [*Brasseur and Solomon*, 2005]. Advection corresponds to the large-scale net motion of air ("residual circulation") and includes also the resolved mixing. Eddy diffusion is transport by turbulence and implies the unresolved and irreversible vertical mixing. Its main source in the mesosphere and lower thermosphere is the breaking of gravity waves. Molecular diffusion is caused by molecular movement and is especially important above 90 km due to the increased path lengths at low densities. Additionally, gravitational settling redistributes molecules vertically according to their molecular mass and is commonly considered as a component of molecular diffusion.

Smith et al. [2011] analyzed the origin of particles in the polar stratosphere in the Whole Atmosphere Community Climate Model (WACCM) by calculating back trajectories from daily values of the Transformed Eulerian Mean circulation. They stated that in most winters, the stratospheric air at high latitudes originates in the upper mesosphere at lower latitudes, from where it was brought to the pole by the mesospheric circulation. Outside the polar vortex, NO_x is destroyed by sunlight, so the horizontal transport cannot explain the large enhancements in stratospheric NO_x concentration observed after times with high geomagnetic activity. *Smith et al.* [2011] also showed that eddy and molecular diffusion can transport high concentrations of thermospheric NO_x to the middle atmosphere, but the roles of the individual transport processes have not yet been quantified. This study aims, for the first time, to quantify the contribution of individual transport process.

Recent studies showed an enhancement of the descent of NO_x after sudden stratospheric warming (SSW) events [*Randall et al.*, 2009; *Holt et al.*, 2013]. The major SSW event in January 2009 was the strongest and most prolonged on record (see *Chandran et al.* [2014] for more information on SSW and especially on the coupling between stratosphere and mesosphere). Anomalous wave-2 activity in the upper troposphere caused a reversal of the NH polar vortex westerlies [*Manney et al.*, 2009]. The stratopause warmed, displaced to a lower level, and finally broke down. Contemporaneously with the warming of the stratosphere, the mesosphere cooled. In early February 2009, the stratopause reformed near 80 km. This reformation of the stratopause at an anomalously high altitude is called an elevated stratopause event [*Chandran et al.*, 2013]. Connected to the SSW, the dynamical conditions changed due to modified gravity wave drag [*Limpasuvan et al.*, 2012]. This led to an unusually strong descent of NO_x to the stratosphere. The NO_x amount which descended from the thermosphere to the stratosphere was 50 times higher than during the average in 2005, 2007, and 2008 [*Randall et al.*, 2009].

Over the last few years, several studies suggested that the atmospheric dynamics have been changed. *Hoffmann et al.* [2011] presented a positive trend in mesospheric gravity wave activity since 1990, which would lead to a positive trend in eddy diffusion. *Emmert et al.* [2012] showed that an increase in the eddy diffusion coefficient (K_{zz}) of 15% per decade brings the COx (CO + CO_2) trend of the National Center for Atmospheric Research global mean model very close to the trend of satellite observations. Hence, both studies suggested a secularly increasing eddy diffusion. Additionally, the magnitude of K_{zz} is not well constrained by observations [*Liu*, 2009; *Collins et al.*, 2011]. A comparison of K_{zz} from the model and recent estimations from observations is provided in section 2. In section 3.3 we investigate the sensitivity of different transport processes to the value of the eddy diffusion coefficient.

This paper determines the transport processes responsible for the descent of NO_x from the thermosphere to the mesosphere for the extended winter 2008/2009 in HAMMONIA. We analyze four different dynamical cases: (a) undisturbed winter conditions during November and December 2008, (b) the sudden stratospheric warming event in January 2009, (c) undisturbed conditions (November and December 2008) with enhanced eddy diffusion, and (d) the sudden stratospheric warming event in January 2009 with enhanced eddy diffusion. The model enables us to separate the contributions of advection, eddy and molecular diffusion on the total transport by switching off the influence of the processes on the tracer. We implement an artificial, passive tracer (i.e., no impact on radiation and dynamics and no interaction with chemistry). Section 2 describes the model setup and evaluates the model by comparing the vertical profile of NO to satellite observations. Section 3 shows the contributions of advection, eddy and molecular diffusion on the total transport as well as the sensitivity of the transport to a SSW event and enhanced eddy diffusion. Finally, section 4 summarizes and discusses the main outcomes and limitations of this study.

2. HAMMONIA: The Hamburg Model of the Neutral and Ionized Atmosphere

HAMMONIA [*Schmidt et al.*, 2006] is a high-top model based on the ECHAM5 atmospheric general circulation model [*Roeckner et al.*, 2006]. The model treats atmospheric dynamics, chemistry, and radiation interactively from the surface to approximately 250 km altitude. The dynamics and radiation are fully coupled to the chemical Model of Ozone and Related Tracers [*Kinnison et al.*, 2007].

To consider the effects of EPP, the HAMMONIA version used in this study is expanded to include the ion chemistry of the ionospheric *E* and *F* regions [*Kieser*, 2011]. The ion chemistry consists of 13 ion-neutral reactions and 5 ion-electron recombinations involving O^+, O_2^+, M^+, N_2^+, NO^+, and electrons. Five reactions directly involving precipitating energetic particles are considered. The ionization of O, O_2, and N_2 is calculated by using the particle-induced ion pair production rates provided by the Atmospheric Ionization Module Osnabrück (AIMOS version 1.6) [*Wissing and Kallenrode*, 2009]. The explicit consideration of energetic particles is limited to the thermosphere, whereas in the middle atmosphere the production of atomic N and HO_x is parameterized following *Jackman et al.* [2005]. The reaction rate coefficient of the 107 trimolecular and bimolecular gas phase reactions used by *Schmidt et al.* [2006] are updated according to *Sander et al.* [2006].

Eddy and molecular diffusion are of central importance for the transport in the upper mesosphere and lower thermosphere. The parameterization of eddy diffusion describes the vertical mixing of air parcels not resolved by the model. In HAMONNIA, eddy diffusion near the mesopause region is almost exclusively caused by

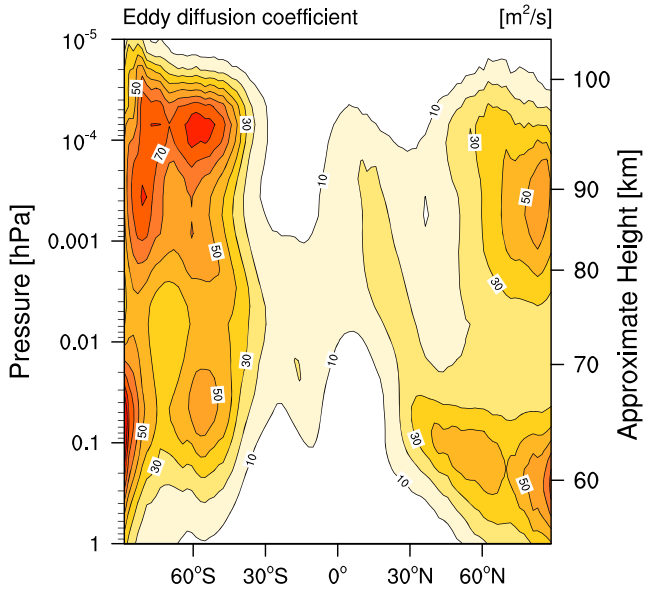

Figure 2. Zonal mean eddy diffusion coefficient from HAMMONIA for November and December 2008. Contour interval is 10 m^2/s.

breaking of gravity waves, which is parameterized according to *Hines* [1997a, 1997b]. Eddy diffusion is given by

$$\frac{\partial X_i}{\partial t} = \frac{1}{\rho}\frac{\partial}{\partial z}\left(\rho K_{zz}\frac{\partial X_i}{\partial z}\right), \tag{1}$$

where ρ is the density (g/m^3), t and z describe the time and vertical dimensions (s and m), X_i is the mass-mixing ratio of the constituent i (kg/kg), and K_{zz} is the respective eddy diffusion coefficient (m^2/s). K_{zz} is a product of the gravity wave parameterization depending on the total root-mean-square of the horizontal wind fluctuation, the rate of energy deposition, and the buoyancy frequency. At altitudes where molecular diffusion is strong, eddy diffusion is limited as suggested by *Akmaev et al.* [1997].

The magnitude of eddy diffusion in the mesopause region is not well constrained by observations. However, several studies indicate that models may underestimate it. Figure 2 shows the zonal mean of K_{zz} from the default version of HAMMONIA for November and December 2008. The winter pole maximum (53 m^2/s) at 0.003 hPa corresponds to gravity wave breaking. Above 10^{-4} hPa the eddy diffusion coefficient rapidly decreases to less than 10 m^2/s. *Smith* [2012] showed a similar figure for WACCM but revealed much smaller values (about 25 m^2/s at 0.001 hPa at the winter pole). *Grygalashvyly et al.* [2011] calculated the diffusivity with a gravity wave-resolving model and estimated magnitudes for K_{zz} of several 100 m^2/s. *Liu* [2009] measured the annual mean eddy diffusion coefficient by a lidar for the winters in 1998–2000 between 100 and 500 m^2/s. *Collins et al.* [2011] derived from lidar measurements a lower boundary of K_{zz} of 430 m^2/s. The values from HAMMONIA are much smaller than any of those estimations. The large differences between different models and observations are still unresolved.

Molecular diffusion is parameterized following the governing equation [*Huang et al.*, 1998]:

$$\frac{\partial X_i}{\partial t} = \frac{1}{\rho}\frac{\partial}{\partial z}\left(\rho D_i\frac{\partial X_i}{\partial z}\right) - \frac{1}{\rho}\frac{\partial}{\partial z}\left(\rho w_{D_i} X_i\right). \tag{2}$$

D_i is the respective molecular diffusion coefficient (m^2/s), and w_{D_i} is the vertical drift velocity, which separates the constituents of different molecular mass. D_i and w_{D_i} for NO_x are taken from *Banks and Kockarts* [1973]:

$$\rho D_i = 4.17\times10^{-6}\left(\frac{T}{273.15K}\right)^{0.5}\left(m_A + \frac{m_A^2}{m_i}\right)^{0.5}, \tag{3}$$

$$\rho w_{D_i} = \frac{\rho D_i g}{R^* T}\left(m_A - m_i\right). \tag{4}$$

T is the temperature (K), g is the gravity acceleration (m/s^2), m_A is the molar mass of air (g/mol), m_i is the molar mass of the constituent i (g/mol), and R^* is the gas constant and is 8.31436 J/(mol K). As we analyze the transport of NO_x, we use its molecular mass. This implies that the difference between m_A and m_i in equations (3) and (4) is small. From this follows that the influence of the vertical drift is negligible compared to molecular diffusion in equation (2). Advection of tracers is performed using the flux form semi-Lagrangian scheme of *Lin and Rood* [1996].

As in the work by *Schmidt et al.* [2010], HAMMONIA is run with 119 vertical levels but with a triangular truncation at wave number 63 (T63) instead of at wave number 31 (T31). This corresponds to a horizontal resolution of 1.9° in longitude and latitude. The vertical resolution is about 800 m in the upper troposphere and stratosphere and about 3 km in the mesopause region.

We carried out four sets of simulations: an ensemble of four simulations for undisturbed conditions running from October 2008 to May 2009 with slightly different initial conditions, a single run for SSW conditions running for January and February 2009, a single run for undisturbed conditions with enhanced eddy diffusion running from October 2008 to January 2009, and a single run for SSW conditions with enhanced eddy diffusion. For undisturbed conditions, the passive tracer is instantaneously emitted on the first time step of each month (e.g., 1 October 2008 at 00:00 A.M.) and for SSW conditions, on 20 January 2009 at 00:00 A.M. The passive tracer is emitted between 80° and 90°N at three different vertical levels: 10^{-2} hPa, 10^{-3} hPa, and 10^{-4} hPa (as shown by the blue dots in Figure 1). The mesopause lies for all simulations near 0.0002 hPa.

Further simulations are created with unchanged dynamics; individual transport processes are switched off (i.e., the influence of the processes on the tracer is switched off). In all of those integrations, the surface pressure, the temperature, the divergence, and the vorticity are nudged (i.e., relaxed) from 850 hPa to 1 hPa with an upper and lower transition zone. The nudging data are 6-hourly values of the European Centre for Medium-Range Weather Forecasts Interim Re-Analysis (ERA-interim) [*Dee et al.*, 2011]. The nudging assures that the model captures the tropospheric and stratospheric dynamics as observed during the extended winter 2008, including the major SSW event in January 2009. As the indirect effect of EPP—and hence the downward transport of NO_x—is most important at the winter polar cap, we concentrate our analysis on the high latitudes and show in all following figures polar cap averages (60°N–90°N).

2.1. Evaluation of the Transport in the Model

Simulations of stratospheric and mesospheric chemistry and dynamics of HAMMONIA at resolution T31 have been compared to observations [e.g., *Dikty et al.*, 2010; *Schmidt et al.*, 2010] and to other models [*Pedatella et al.*, 2014]. The model performs well in simulating the climatological mean values of temperature, winds, and most chemical species in the stratosphere and mesosphere. The High Energy Particle Precipitation in the Atmosphere model versus Michelson Interferometer for Passive Atmospheric Sounding (MIPAS) [*Fischer et al.*, 2008] data intercomparison study [*Funke et al.*, 2011] provides a detailed evaluation on the ability of several general circulation models (including HAMMONIA) and chemistry transport models to simulate EPP effects. HAMMONIA revealed too strong horizontal mixing across the polar vortex boundaries due to continuous wave-1 activity. The polar winter descent of CO is well reproduced in HAMMONIA. The stratospheric and mesospheric ozone response to the "Halloween storms" in October and November 2003 is well simulated in terms of temporal evolution and latitudinal distribution. However, the midterm ozone loss (between 16 and 26 November 2003) is too weak in HAMMONIA. Differences between our simulations at T63 horizontal resolution are small with respect to the previously used model version at T31 resolution (not shown).

Realistic transport of NO_x in the middle atmosphere is critical for our analysis. We compare the vertical profiles of NO in the mesosphere and lower thermosphere to MIPAS (see Figure 3). Several studies have shown the excellent agreement between MIPAS and other satellite observations—e.g., the Atmospheric Chemistry Experiment Fourier Transform Spectrometer (ACE-FTS) [*Garcia et al.*, 2014; *Bender et al.*, 2014]. Hence, a comparison to ACE-FTS yields similar results as the comparison to MIPAS.

We interpolate 2-hourly gridded HAMMONIA data to the actual measurement times and locations of MIPAS. For the error estimates of MIPAS, we followed the approach of *Garcia et al.* [2014] and assume 10% systematic error and use one sigma of the standard error, which is calculated from the averaging over the polar cap. The total error is then the sum in quadrature of the systematic and standard error.

The NO profile simulated with HAMMONIA using the standard eddy diffusion coefficient (1 × Kzz) is denoted by the red line in Figure 3. The increase of NO in the mesosphere is well reproduced by the model;

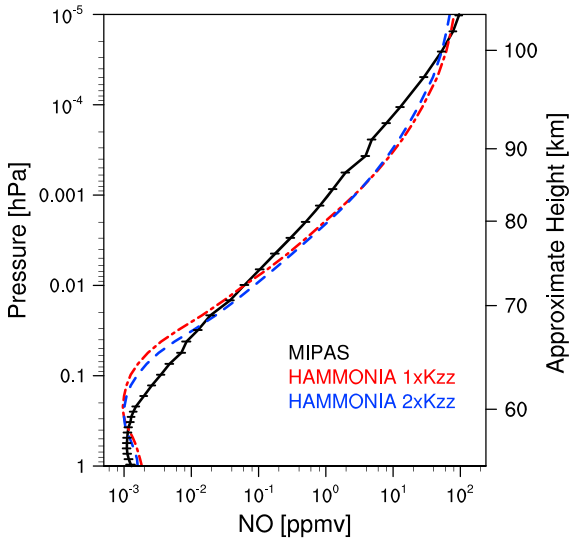

Figure 3. Vertical profiles of NO volume mixing ratio for November and December 2008 in HAMMONIA (colored lines) and in MIPAS (black line) averaged over the polar cap (60° – 90°N). Two experiments of HAMMONIA with different eddy diffusion coefficients are shown: 1 × Kzz (dash-dotted, red) and 2 × Kzz (dashed, blue). The error bars represent the total error (i.e., the sum in quadrature of the systematic error and the standard error of the area averaging).

however, we find some differences. HAMMONIA shows a local minimum near 0.2 hPa, and the rate of increase of NO with increasing height is slightly higher in the model than in the observations. This implies too little NO around 0.2 hPa and too much NO above 0.01 hPa in HAMMONIA.

The underestimation at 0.2 hPa has also been found in other models covering this altitude region and may be related to an overestimation of NO photolysis, which is a major NO loss mechanism in the illuminated mesosphere [*Funke et al.*, 2011]. This is also supported by the fact that the underestimation shrinks if we average over 70° – 90°N, where the loss mechanism is weak (not shown). However, we cannot exclude the influence of overestimated mixing of polar and midlatitude air masses. The overestimation above 0.01 hPa may be related to the use of AIMOS, as it does not use the corrected medium energy electrons from the POES MEPED (Polar-orbiting Operational Environmental Satellites Medium Energy Proton/Electron Detector) instrument. This can result in an overestimation of ionization — and hence, NO — in the lower thermosphere and upper mesosphere [*Peck et al.*, 2015; *Rodger et al.*, 2010]. There is an overall good agreement between MIPAS and HAMMONIA. Differences are between 10% and 20% below 0.1 hPa. The largest discrepancies emerge between 0.001 and 10^{-4} hPa, where the model overestimates the concentration of NO by 100%.

3. Results

In the following, we analyze the transport of NO_x from the thermosphere to the mesosphere by switching on only individual transport processes for the passive tracer. We concentrate on four different dynamical cases: (1) undisturbed conditions (November and December 2008), (2) SSW conditions (January and February 2009), (3) undisturbed conditions with doubled eddy diffusion coefficient (November and December 2008), and (4) SSW conditions with doubled eddy diffusion coefficient (January and February 2009). For each case the same two subfigures are presented, which we introduce here briefly.

Figures 4a, 4c, 4e, and 4g show the vertical distribution of the passive tracer 30 days after emission. Only individual transport processes are switched on (M = molecular diffusion, E = eddy diffusion, A = advection), while effects of the respective other processes on the tracer distribution are switched off. Figure 4a corresponds to undisturbed conditions, 4c to the SSW conditions, 4e to undisturbed conditions with 2 × Kzz, and 4g to SSW conditions with 2 × Kzz. In the model, molecular and eddy diffusion only act in the vertical, while advection also transports horizontally. To consider that the processes transport the tracer over different latitudinal bands, the tracer mass $\tilde{\chi}$ is normalized against the total tracer mass between 60° and 90°N at day 30 after emission (t_{end}):

$$\chi(t,z,\phi) = \frac{\tilde{\chi}(t,z,\phi)}{\int_{z=0}^{Z}\int_{\phi=60°N}^{90°N}\tilde{\chi}(t_{end},z,\phi)}. \quad (5)$$

χ is the normalized tracer mass as a function of time t, altitude z, and latitude ϕ. A value of 1 kg/kg would correspond to all mass being stored in a single layer after 30 days; hence, no transport occurs. Note that the

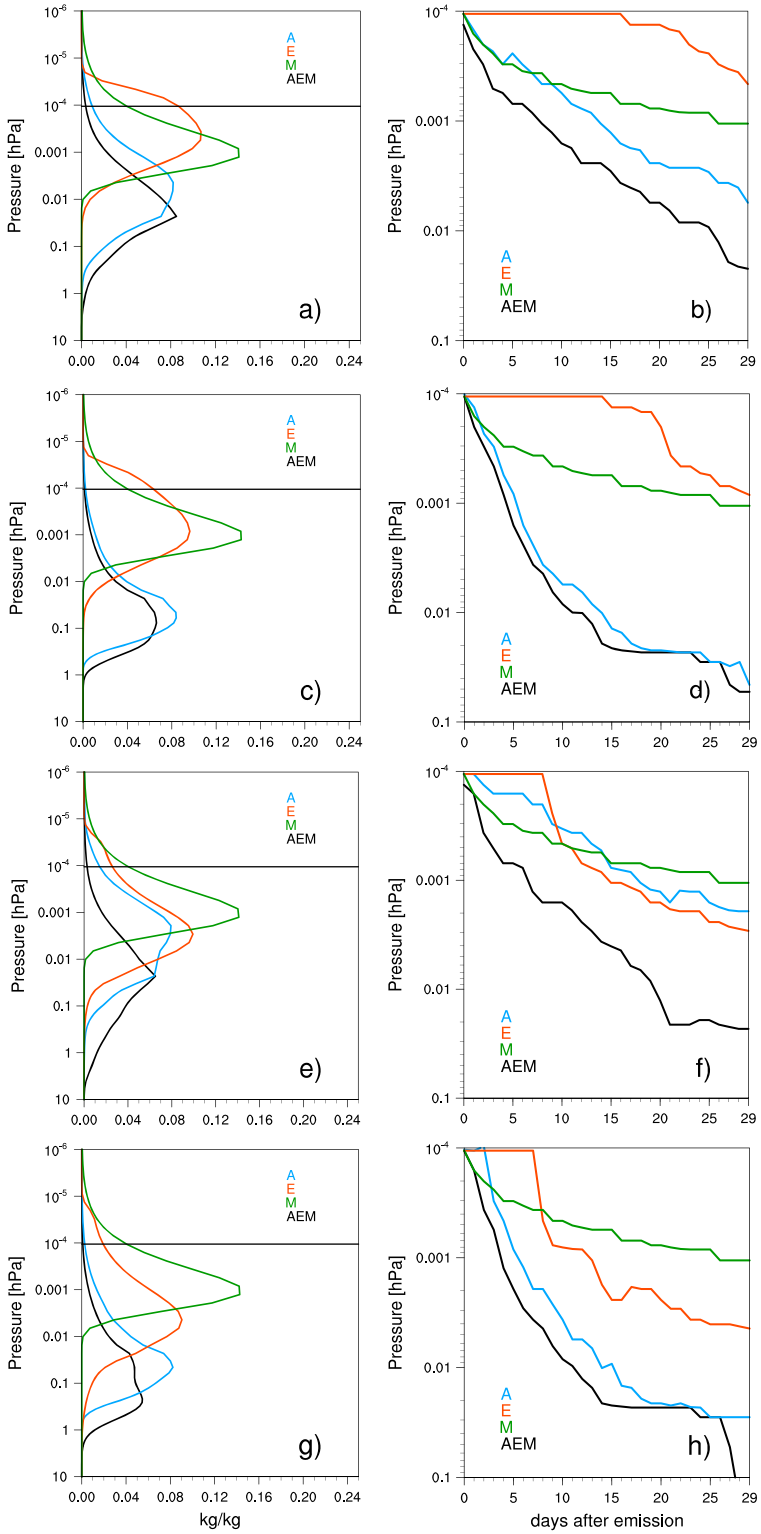

Figure 4. (left column) Normalized tracer mass 30 days after emission averaged over 60°–90°N. The horizontal line is the emission height at 10^{-4} hPa. (right column) Vertical trajectory of the tracer maximum (kg/kg) over 60°–90°N. Individual transport processes are switched on (A = advection, M = molecular diffusion, E = eddy diffusion, AEM = control simulation with all processes switched on. (a, b) For undisturbed conditions (November and December 2008), (c, d) for SSW conditions (January 2009), (e, f) as for Figures 4a and 4b but with 2 × Kzz, and (g, h) as for Figures 4c and 4d but with 2 × Kzz. We use the ensemble mean for Figures 4a and 4b and a single run for all others. The tracer is emitted on the first day of each month, except for Figures 4c, 4d, 4g, and 4h where the tracer is emitted on 20 January 2009.

normalized tracer mass provides no information on the actual transported tracer mass. Henceforward, we only use the normalized tracer mass but refer to it for simplicity as tracer mass.

Figures 4b, 4d, 4f, and 4h show the vertical trajectory of the tracer maximum as a function of time and altitude. For each day the height of the maximum in the (normalized) tracer mass is estimated. Again, only individual transport processes are switched on (M = molecular diffusion, E = eddy diffusion, A = advection). Figure 4b corresponds to undisturbed conditions, 4d to SSW conditions, 4f to undisturbed conditions (as 4b) but with $2 \times$ Kzz, and 4h to SSW conditions (as 4d) but with $2 \times$ Kzz. As the tracer maximum is calculated with discrete model levels, this can create a step function artifact (compare to the red line in Figure 4b). Additionally, we only show one aspect of the distribution (i.e., the level of the maximum). Hence, the distribution may spread even if the tracer maximum remains at one level.

3.1. Undisturbed Winter Conditions

In this section, we analyze the impact of different transport processes for undisturbed conditions. First, we explore the vertical distribution of the passive tracer 30 days after emission (see Figure 4a). We use the ensemble mean of four ensemble members and average over November and December 2008. Due to the nudging up to 1 hPa, the differences between the individual ensemble members are negligible. To prove this, we calculate the maximum deviation of the ensemble mean (maximum spread − minimum spread for all emissions levels and processes). The maximum spread is 0.03 kg/kg at 0.01 hPa, which is smaller than the line thickness in Figure 4a. Analyzing November and December 2008 assures relatively undisturbed winter conditions. If the tracer is emitted on the first of each month, the months October 2008 to February 2009 show a similar behavior as November and December 2008. In section 3.2 we analyze the transport during the SSW in January 2009 by emitting the tracer on 20 January 2009.

If only molecular diffusion is switched on, most of the tracer mass emitted at 0.001 hPa and 0.01 hPa is still located near the emission height after 30 days (not shown). The impact of molecular diffusion on the transport below the mesopause region is negligible. Eddy diffusion behaves similarly when the tracer is emitted at 0.01 hPa but not as extreme as molecular diffusion, i.e., advection is the dominant process at this altitude range. In the upper mesosphere, eddy diffusion is the second most important process, but the impact of advection is considerably larger. Hence, below the mesopause region, advection is the dominating transport process. This is in line with the results of *Smith et al.* [2011] and agrees well with our expectations, because at this altitude range the mesospheric circulation has a descending branch over the winter pole (see Figure 1).

However, for single events with large thermospheric NO_x source, e.g., an EPP event, the transport from the thermosphere to the mesosphere cannot be neglected. In the lower thermosphere, all three processes contribute to the transport (see Figure 4a), but the relative importance of the processes varies. While molecular diffusion and advection bring the tracer maximum down below the mesopause, most of the tracer transported by eddy diffusion remains above 0.001 hPa. The strong impact of advection disagrees with our expectations from Figure 1.

However, the shown stream function is the mean over 2 months, while on intradiurnal time scale (i.e., within a day) the variability is high. To illustrate this, we calculate the intradiurnal (from 6-hourly output) and day-to-day (from daily means of the 6-hourly output) standard deviation of the zonal mean residual vertical wind (w^*) averaged between 0.001 and 10^{-4} hPa and between 60° and 90°N for November and December 2008. The intradiurnal variability (0.022 m/s) is 3 times larger than the day-to-day variability (0.007 m/s). This behavior is also evident in the averages over individual universal times (i.e., the mean over all time steps at 0, 6, 12, and 18 UT in November and December 2008): The 6 UT mean (−0.0127 m/s) and the 18 UT mean (−0.0196 m/s) show strong descent, while the 0 UT mean (0.0073 m/s) and the 12 UT mean (0.0082 m/s) show ascent. The intradiurnal variability strongly affects the downward transport of NO. Figure 5 shows the change in NO concentration due to the TEM residual vertical wind calculated from (a) the 6-hourly model output and (b) the daily mean as the average over the 6-hourly time steps. In the lower thermosphere the impact of the residual vertical wind on the NO concentration is doubled when 6-hourly values are used. We speculate that the influence of the large intradiurnal variability on the transport of NO is caused due to the dynamical transport by atmospheric tides as described in *Jones et al.* [2014] for lower latitudes. However, sensitivity studies with more idealized models would be needed to confirm this.

This resolved vertical mixing (as well as the mixing by molecular diffusion) balances the gradient of the mass-mixing ratio, which leads to a higher amount of mass below than above the emission level due to

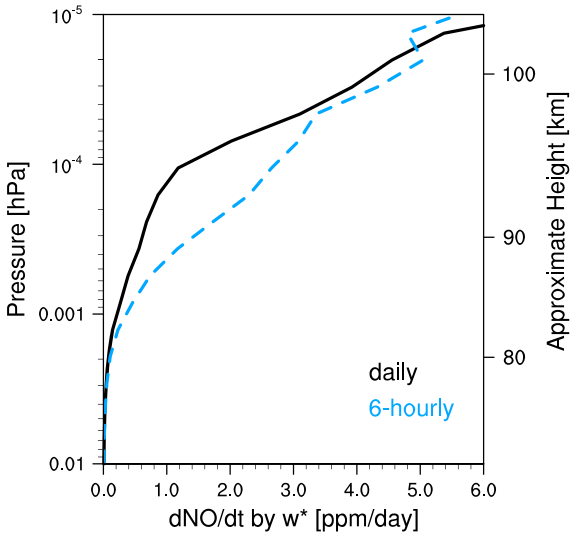

Figure 5. Tendency of NO concentration (ppm/day) due to advection by the residual vertical wind averaged over 60° – 90°N calculated from 6-hourly output (blue dashed line) and from the daily mean as the average over the 6-hourly output (black solid line). This is a diagnostic variable computed by the TEM analysis.

the decrease in density with increasing height. As mentioned above, all three processes act on the tracer (i.e., transport the tracer maximum downward), but Figure 4a is only a snapshot, i.e., it shows the distribution of the tracer only at one time step (day 30 after emission). Hence, the initial impact of individual processes in the lower thermosphere is masked.

For a better understanding of the behavior in the lower thermosphere, we separate the impact of advection, eddy and molecular diffusion for single model levels. Figure 4b shows the vertical trajectory of the tracer maximum for different processes. In the highest model levels, transport by advection and by molecular diffusion have the same order of magnitude and the maximum concentration of the tracer is transported by advection and molecular diffusion within 8 days to $3.6 \cdot 10^{-4}$ hPa. The tracer maximum transported by eddy diffusion remains for 17 days at the emission level before it reaches the next lower level. Hence, eddy diffusion has a negligible impact on the transport in the lower thermosphere in this case. At altitudes below $4.6 \cdot 10^{-4}$ hPa, advection dominates the transport. While molecular diffusion is still second most important down to 0.001 hPa, its impact on the transport decreases below and eddy diffusion becomes the second largest process (not shown).

As mentioned above, the increasing influence of advection with decreasing height is not surprising because of the generally downward circulation in the high-latitude winter mesosphere. The impact of molecular diffusion is very similar for all months and does not depend on dynamical conditions. The major source of eddy diffusion in the middle and upper atmosphere is the breaking of gravity waves in the upper mesosphere. The step function of the trajectory due to eddy diffusion is associated with the strong gradient of the tracer at the emission level. As mentioned above, Figure 4b shows only the level of the maximum, which can only have discrete model levels. A sudden height change in the tracer maximum may have been caused by a flat distribution of the tracer. A small vertical redistribution of the tracer mass then may lead to a rapid (vertical) displacement of the tracer maximum. The eddy diffusion coefficient is relatively small at 10^{-4} hPa (see Figure 2) and about 6 times smaller than the molecular diffusion coefficient (not shown). Hence, it takes 17 days until eddy diffusion mixes enough tracer from the emission level so that a new maximum develops below. We analyze this behavior more in detail in section 3.3.

3.2. Impact of the Sudden Stratospheric Warming Event in January 2009

In the following, we investigate how the SSW in January 2009 influences the transport of NO_x from the thermosphere to the stratosphere. Figure 4c shows the vertical distribution of the passive tracer after 30 days. The passive tracer is emitted on 20 January 2009, shortly before the SSW. We compare Figures 4a and 4c to determine whether transport processes act differently during a SSW versus during undisturbed conditions.

Results shown here indicate that the downward transport of the tracer by eddy and molecular diffusion are similar to those during undisturbed winter conditions. While the maximum concentration of the tracer transported by eddy diffusion remains at roughly the same altitude, the distribution slightly broadens. The SSW has little influence on eddy and molecular diffusion. Advection strengthens in the lower thermosphere and upper mesosphere. Irrespective of the emission height, the maximum of the tracer transported by advection reaches 0.1 hPa. Under undisturbed winter conditions, the tracer emitted at 10^{-4} hPa is after 30 days at a much higher altitude (about 0.01 hPa), while the tracer emitted at 0.01 hPa reaches much further down (about 10 hPa, not shown) (see Figures 4a and 4c). Hence, during SSW conditions the descent rate of the tracer slows down below 0.1 hPa.

Table 1. Intermonthly Spread of the Endpoints of the Trajectories of the Tracer Maximum (hPa) for Undisturbed Conditions (October 2008 to February 2009) and Endpoints of the Trajectories of the Tracer Maximum (hPa) for SSW Conditions (January and February 2009), Undisturbed Conditions With 2 × Kzz (November and December 2008), and SSW Conditions With 2 × Kzz (January and February 2009)[a]

Case	AEM	A	E
Undisturbed conditions (min–max)	0.0150–0.0254	0.0030–0.0222	0.0002–0.0012
SSW conditions	0.0530	0.0457	0.0008
Undisturbed conditions with 2 × Kzz	0.0231	0.0019	0.0029
SSW conditions with 2 × Kzz	0.2178	0.0283	0.0044

[a]Single transport processes are switched on (A = advection, E = eddy diffusion, AEM = control simulation with all processes switched on).

The analysis of the tracer maximum in Figure 4d confirms the small impact of eddy and molecular diffusion on the transport during the SSW. The tracer maximum transported by eddy diffusion reaches the next lower discrete model level slightly earlier (after 15 days compared to after 17 days during undisturbed winter conditions). Changes in eddy diffusion are due to the strong circulation changes, which affect the propagation conditions of gravity waves [*Limpasuvan et al.*, 2012]. However, eddy diffusion is still the weakest process above 0.001 hPa. Advection is much stronger than under undisturbed winter conditions. In 8 days, the tracer maximum reaches 0.0024 hPa compared to $3.6 \cdot 10^{-4}$ hPa under undisturbed conditions. The deceleration in the downward transport below 0.1 hPa is confirmed by Figure 4d.

To evaluate the robustness of these results, we compare the intermonthly spread of the endpoints of the trajectories for undisturbed winter conditions to the endpoints of the trajectories for SSW conditions (see Table 1). The intermonthly spread (minimum and maximum of the endpoints over all months) describes how strongly the endpoints of each trajectory vary between the months in height. The comparison of the intermonthly spread to the endpoints of each trajectory during SSW conditions shows how different the results for SSW conditions are from the results for undisturbed conditions. The intermonthly spread is calculated for the control tracer (AEM—all processes switched on), the tracer transported by eddy diffusion (E), and the tracer transported by advection (A) using October 2008 to February 2009. We did not calculate the ensemble spread for the tracer transported by molecular diffusion as it does not depend on the dynamics and hence its trajectories are very similar for all months and all dynamical conditions. Table 1 shows that the endpoints for SSW conditions are outside the intermonthly spread for the control tracer and the tracer transported by advection, which indicates a robustly different behavior under SSW conditions.

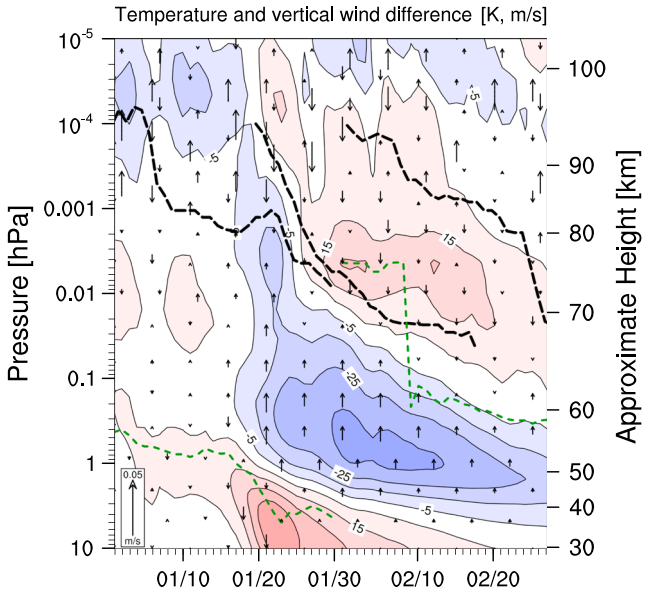

Figure 6. Temperature (colored contours) and residual vertical wind (vectors) differences (K, m/s) between January and March 2009 and the mean over November and December 2008. The dashed lines correspond to the vertical trajectory of the tracer maximum transported by advection only. Three emission times are shown: 1 January, 20 January, and 1 February (from left to right). The dashed green line represents the height of the stratopause. The contour interval is 10 K.

Figure 6 shows the temperature and residual vertical wind differences for January to mid-February 2009. The differences are calculated with respect to the mean of November and December 2008. The height of the stratopause (dashed green line) is determined as the first local temperature maximum above the tropopause. The warming and displacement of the stratopause to a lower altitude is well reproduced.

In early February, the stratopause reforms at high altitudes above 80 km. However, the reformation and the descent of the elevated stratopause happen too quickly, which is common in models covering this altitude range [*Pedatella et al.*, 2014]. The vertical residual wind differences explain well the trajectories of the tracer maximum (dashed lines). Note that only the tracer transported by advection is shown but for three different emission times. Strong downwelling occurs during the warming in the upper mesosphere, which is related to the elevated stratopause and its descent to its climatological altitude [*Chandran et al.*, 2013]. Note that there is no net upward flow between 10 and 0.1 hPa after the SSW but just weakened downward flow. The weak descent of the tracer below 0.1 hPa seen in Figures 4c and 4d is caused by convergent winds at 0.03 hPa.

Direction and strength of advection are highly variable on the time scale of a few days during the period of the SSW. *Holt et al.* [2013] stated that the amount of stratospheric NO_x varies with the timing of a SSW event within a season. The earlier the event occurs in the winter, the more NO_x is transported to the stratosphere. The strong dependency of stratospheric NO_x on the timing of SSW has two main reasons: (1) the earlier the SSW occurs, the more negative (descent) is the vertical wind, and (2) the earlier the SSW occurs, the longer the NO_x descends and the less NO_x is mixed laterally (due to the breakdown of the polar vortex) to latitudes, where it gets destroyed by sunlight. *Holt et al.* [2013] used a constant EPP forcing during the whole simulation, i.e., a continuous auroral electron EPP event. We find that the descent of NO_x varies in terms of velocity and mass over a few days during the SSW. Hence, the amount of stratospheric NO_x depends not only on the timing of the SSW within the winter season but also on the timing of the EPP forcing (production of NO_x) and of the disturbed SSW dynamics on the time scale of a few days.

3.3. Impact of a Doubled Eddy Diffusion Coefficient

Garcia et al. [2014] suggested an underestimation of eddy diffusion in WACCM (version 4). They increased K_{zz} by halving the Prandtl number, which is inversely proportional to K_{zz}. For doubled K_{zz}, WACCM agrees better with the observations for CO_2. The default value of the Prandtl number used in HAMMONIA is 3, which is between the standard value used in WACCM (Pr = 4) and the tuned value (Pr = 2) used by *Garcia et al.* [2014]. In the following, we investigate the effect of a stronger eddy diffusion on the downward transport. To estimate the consequences of such an underestimation or of changes over time, we doubled the eddy diffusion coefficient ($2 \times$ Kzz) in the gravity wave parameterization scheme (see section 2 and equation (1) for more details on the implementation of eddy diffusion in HAMMONIA).

As for $1 \times$ Kzz, we investigate the vertical distribution of the passive tracer averaged over November and December 2008 (see Figure 4e), but for $2 \times$ Kzz we only use one ensemble member. The distribution of the tracer transported by advection slightly changes compared to $1 \times$ Kzz (see Figure 4a), while eddy diffusion clearly strengthens at all altitudes but most in the lower thermosphere. For $1 \times$ Kzz, the maximum of the tracer transported by eddy diffusion is at $3 \cdot 10^{-4}$ hPa for the emission level of 10^{-4} hPa and 0.003 hPa for the emission level of 0.001 hPa (not shown). For $2 \times$ Kzz, the tracer maximum is transported further down: 0.003 hPa for the emission level of 10^{-4} hPa and 0.007 hPa for the emission level of 0.001 hPa (not shown). Below the mesopause region, advection is still the dominant process and eddy diffusion the second largest process (not shown).

Figure 4f shows the vertical trajectory of the tracer maximum for $2 \times$ Kzz for the mean over November and December 2008. Advection is much weaker than for $1 \times$ Kzz (see Figure 4b). A change in K_{zz} may influence advection, because nonresolved vertical mixing acts not only on composition but also on momentum. Further analysis of the relation between K_{zz} and advection is beyond the scope of this study. With a weaker advection, molecular diffusion is the leading process for the total transport down to about $5 \cdot 10^{-4}$ hPa. Note that, as mentioned before, molecular diffusion only weakly depends on the dynamics and its impact on the transport is, hence, the same as under undisturbed winter conditions. After 9 days the tracer transported by eddy diffusion develops a new maximum below the emission level. For $1 \times$ Kzz, the tracer maximum transported by eddy diffusion remains 17 days at the emission level before building a new maximum below. Hence, the time until a new tracer maximum is developed below the emission level is almost halved for $2 \times$ Kzz. Furthermore, the transport by eddy diffusion is strongly enhanced in the lower thermosphere and upper mesosphere. Between $5 \cdot 10^{-4}$ hPa and 0.003 hPa eddy diffusion is dominant, while advection takes over below 0.003 hPa (not shown). Eddy diffusion can potentially have a large impact on the transport to the mesosphere. However, the impact of eddy diffusion depends on K_{zz}, which bears a large uncertainty.

To evaluate the robustness of our results, we compare the endpoints of each trajectory for $2 \times$ Kzz to the intermonthly spread of the ensemble for $1 \times$ Kzz (see Table 1). This comparison describes whether the results of $2 \times$ Kzz are different from the intermonthly changes of $1 \times$ Kzz. A more detailed description on how the

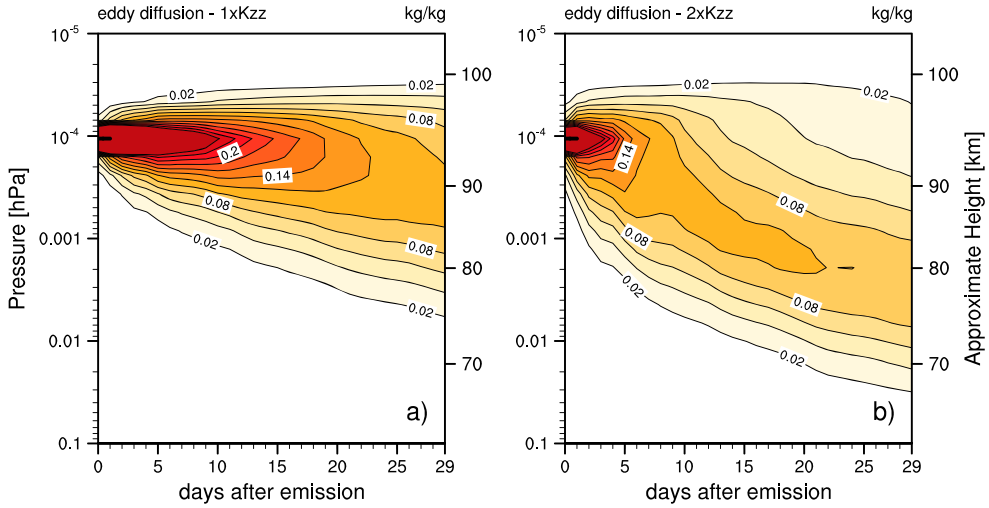

Figure 7. Normalized tracer mass transported only by eddy diffusion for undisturbed conditions with (a) 1 × Kzz and (b) 2 × Kzz. The average of the simulations with emission dates on 1 November and 1 December 2008 are shown. We use the ensemble mean for Figure 7a and a single run for Figure 7b. The tracer is emitted at the first day of each month. The contour interval is 0.02 kg/kg.

intermonthly spread is calculated is provided in section 3.2. Table 1 shows that the endpoints for 2 × Kzz are outside the intermonthly spread for the tracer transported by advection and by eddy diffusion, which indicates a robustly different behavior for 2 × Kzz.

To test if the impact of an enhanced eddy diffusion changes during disturbed SSW dynamics, we have performed an additional experiment with 2 × Kzz during SSW conditions (see Figures 4g and 4h). We find that the strengthening of advection due to SSW dynamics is larger than the strengthening of eddy diffusion due to doubled K_{zz}. The endpoint of each trajectory lies outside the intermonthly spread of the ensemble for undisturbed conditions with 1 × Kzz (see Table 1).

Figure 7 shows the normalized tracer mass transported only by eddy diffusion as a function of altitude and time. Only the tracer emitted at 10^{-4} hPa is shown. The mean over November and December 2008 for two different K_{zz} values is used, (a) for 1 × Kzz and (b) for 2 × Kzz. The tracer maximum remains for both K_{zz} values several days at the emission level; however, the distribution spreads. For both K_{zz} values, a flat distribution develops around the tracer maximum. If a small amount of mass is then transported downward from the emission level, a new maximum develops several levels below. This happens for 1 × Kzz at day 17 and for 2 × Kzz at day 9 and explains the sudden descent of the tracer maximum seen in Figures 4b and 4f. For 2 × Kzz, eddy diffusion is much stronger, and hence, the strong gradient at the emission level is weakened faster. This leads to the earlier descent of the tracer maximum for 2 × Kzz.

To evaluate the influence of an enhanced eddy diffusion on the transport, we compare NO profiles simulated with 2 × Kzz to the MIPAS data (see Figure 3). As in the reference simulation, also the simulation with doubled K_{zz} underestimates the concentration of NO at 0.1 hPa and overestimates it above 0.01 hPa. Doubling the eddy diffusion coefficient yields little to no improvement. The largest discrepancies emerge between 0.001 and 10^{-4} hPa, where the model overestimates the concentration of NO by 100%. For CO the agreement between HAMMONIA and MIPAS worsens with 2 × Kzz (not shown), which has also been observed by *Garcia et al.* [2014].

4. Summary and Conclusion

In this study, we analyzed the role of advection, molecular diffusion, and eddy diffusion for the transport of nitrogen oxides through the mesopause region. Simulations with HAMMONIA were carried out including a passive tracer and selected transport processes switched off. We found that molecular diffusion and advection are the dominant processes for the transport of NO_x in the lower thermosphere. The impact of molecular diffusion rapidly decreases with decreasing heights, while the impact of advection increases. Above the mesopause, the intradiurnal variability associated with atmospheric tides strongly affects the transport of NO_x. The dominant impact of advection below the mesopause agrees well with the stream function

theory and other studies [*Smith et al.*, 2011]. In the default configuration of the model, eddy diffusion negligibly contributes to the total transport in the lower thermosphere and weakly contributes to the transport in the upper mesosphere. The weak influence of eddy diffusion on the transport in the thermosphere is caused by a strong gradient of the tracer at the emission level and a small eddy diffusion coefficient.

Besides undisturbed winter conditions, we also analyzed the transport during the sudden stratospheric warming (SSW) in January 2009. Shortly after the SSW, advection is strongly enhanced in the thermosphere and mesosphere, which agrees with the results of *Randall et al.* [2009]. Hence, the downward transport through the mesopause region is dominantly driven by advection. Weak downward residual circulation related to a warming in the upper mesosphere hinders the further descent of the tracer below 0.1 hPa. Over a few days during the SSW advection strongly varies in terms of strength and direction. Hence, the stratospheric amount of NO_x depends strongly on the timing of thermospheric NO_x production due to EPP and disturbed vortex dynamics.

Smith et al. [2011] showed that most air in the polar stratosphere in WACCM originates in the mesosphere at lower latitude, instead of being advected from the thermosphere. Our study agrees on the importance of advection for the downward transport below the mesopause region. However, we did not consider the latitudinal transport and concentrated on the vertical transport. For single events with large thermospheric NO_x source, e.g., an EPP event, the transport from the thermosphere to the mesosphere cannot be neglected. Additionally, *Smith et al.* [2011] considered only daily means, while we have shown that more NO in the lower thermosphere is transported downward if 6-hourly values are taken into account. Thus, this paper extends the analysis of *Smith et al.* [2011] and identifies molecular diffusion and vertical advection as the major drivers for transport in the lower thermosphere for undisturbed winter conditions.

Recent studies have suggested positive trends in eddy diffusion of 15% on the decadal time scale [*Hoffmann et al.*, 2011; *Emmert et al.*, 2012]. We conducted an experiment with doubled eddy diffusion coefficient ($2 \times$ Kzz) to quantify the sensitivity of different transport processes to the value of K_{zz}. In this sensitivity study, eddy diffusion becomes the second largest process for the downward transport in the lower thermosphere and near 0.001 hPa eddy diffusion is dominant. The impact of advection on transport in the lower thermosphere decreases with doubled K_{zz}, leaving molecular diffusion the dominant process. If eddy diffusion is enhanced as suggested by observations or due to a positive trend in K_{zz}, eddy diffusion can potentially have a larger impact on transport through the mesopause region than was previously assumed.

This study is based on the extended winter 2008/2009 and on simulations with HAMMONIA. We evaluated the model with MIPAS observations and find that the model underestimates the vertical gradient of NO concentration in the MLT region, which leads to a slight overestimation of the NO concentration in the lower thermosphere. In the upper mesosphere and lower thermosphere, the simulated NO concentrations are outside of the error bars of the observations. The underestimation of NO in the upper mesosphere (at 0.2 hPa) may be related to an overestimation of the NO photolysis in the illuminated mesosphere. The overestimation of NO in the lower thermosphere (above 0.001 hPa) may be caused by the use of AIMOS, which does not use the corrected medium energy electrons from the POES MEPED instrument [*Peck et al.*, 2015; *Rodger et al.*, 2010]. We believe that the transport is reasonably reproduced by the model. Enhancing eddy diffusion yields only slightly better agreement with MIPAS. Further work on the uncertainty concerning transport processes introduced by the uncertainty of eddy diffusion is needed.

More in general, it is clear that current models cannot reproduce perfectly the observed trace gas distributions indicating deficiencies in the implemented processes. But trace gas observations by satellite only provide insight in the integrated effects of production and transport processes. Estimates of the relative importance of the differences will therefore always rely on modeling efforts. To reduce the uncertainty left by our study, we can imagine two pathways: (1) improving the understanding of the underlying processes and its representation and (2) using observations of specific events that may be more informative concerning transport processes. With respect to (1) observations of gravity wave breaking and the resulting turbulence may allow for improving the representation of both eddy-diffusive and advective transport in models. Gravity wave observation from satellite as suggested by *Geller et al.* [2013] may be one element of such a strategy. With respect to (2) observing the time evolution of trace gas distributions after events of extreme geomagnetic activity may help to better evaluate and constrain numerical models. However, higher temporal and spatial resolution observations are required than currently exist.

Acknowledgments
The authors acknowledge scientific and practical input from Bernd Funke, Angela Gardini, Elisa Manzini, Matthew Toohey, and Bjorn Stevens. This study was supported by the Max-Planck-Gesellschaft (MPG), and computational resources were made available by Deutsches Klimarechenzentrum (DKRZ) through support from Bundesministerium für Bildung und Forschung (BMBF). The Michelson Interferometer for Passive Atmospheric Sounding (MIPAS) is a core mission by the European Space Agency. The authors gratefully acknowledge the "Atmospheres of the terrestrial planets" group of the Instituto de Astrofísica de Andalucía for providing MIPAS data. Katharina Meraner acknowledges support from COST ActionES1005. The work has benefited from discussions within the ISSI team on coupling stratospheric warming led by Nick Pedatella. The authors thank three anonymous reviewers for their helpful comments. Primary data and scripts used in the analysis and other supplementary information that may be useful in reproducing this work are archived by the Max Planck Institute for Meteorology and can be obtained by contacting publications@mpimet.mpg.de.

References

Akmaev, R. A., V. A. Yudin, and D. A. Ortland (1997), SMLTM simulations of the diurnal tide: Comparison with UARS observations, *Ann. Geophys.*, *15*(9), 1187–1197, doi:10.1007/s00585-997-1187-7.

Banks, P. M., and G. Kockarts (1973), *Aeronomy, Part B*, Academic Press, New York.

Bender, S., M. Sinnhuber, T. von Clarmann, G. Stiller, B. Funke, M. López-Puertas, J. Urban, K. Pérot, K. A. Walker, and J. P. Burrows (2014), Comparison of nitric oxide measurements in the mesosphere and lower thermosphere from ACE-FTS, MIPAS, SCIAMACHY, and SMR, *Atmos. Meas. Tech. Discuss.*, *7*(12), 12,735–12,794, doi:10.5194/amtd-7-12735-2014.

Brasseur, G. P., and S. Solomon (2005), *Aeronomy of the Middle Atmosphere: Chemistry and Physics of the Stratosphere and Mesosphere*, Springer, Dordrecht, Netherlands.

Chandran, A., R. L. Collins, R. R. Garcia, D. R. Marsh, V. L. Harvey, J. Yue, and L. de la Torre (2013), A climatology of elevated stratopause events in the whole atmosphere community climate model, *J. Geophys. Res. Atmos.*, *118*, 1234–1246, doi:10.1002/jgrd.50123.

Chandran, A., R. L. Collins, and V. L. Harvey (2014), Stratosphere-mesosphere coupling during stratospheric sudden warming events, *Adv. Space Res.*, *53*(9), 1265–1289, doi:10.1016/j.asr.2014.02.005.

Collins, R. L., G. A. Lehmacher, M. F. Larsen, and K. Mizutani (2011), Estimates of vertical eddy diffusivity in the upper mesosphere in the presence of a mesospheric inversion layer, *Ann. Geophys.*, *29*(11), 2019–2029, doi:10.5194/angeo-29-2019-2011.

Crutzen, P. J., I. S. A. Isaksen, and G. C. Reid (1975), Solar proton events: Stratospheric sources of nitric oxide, *Science*, *189*(4201), 457–459, doi:10.1126/science.189.4201.457.

Dee, D. P., et al. (2011), The ERA-interim reanalysis: Configuration and performance of the data assimilation system, *Q. J. R. Meteorol. Soc.*, *137*(656), 553–597, doi:10.1002/qj.828.

Dikty, S., H. Schmidt, M. Weber, C. von Savigny, and M. G. Mlynczak (2010), Daytime ozone and temperature variations in the mesosphere: A comparison between SABER observations and HAMMONIA model, *Atmos. Chem. Phys.*, *10*(17), 8331–8339, doi:10.5194/acp-10-8331-2010.

Emmert, J. T., M. H. Stevens, P. F. Bernath, D. P. Drob, and C. D. Boone (2012), Observations of increasing carbon dioxide concentration in Earth's thermosphere, *Nat. Geosci.*, *5*(12), 868–871, doi:10.1038/ngeo1626.

Fischer, H., et al. (2008), MIPAS: An instrument for atmospheric and climate research, *Atmos. Chem. Phys.*, *8*(8), 2151–2188, doi:10.5194/acp-8-2151-2008.

Funke, B., M. López-Puertas, S. Gil-López, T. von Clarmann, G. P. Stiller, H. Fischer, and S. Kellmann (2005), Downward transport of upper atmospheric NO_x into the polar stratosphere and lower mesosphere during the antarctic 2003 and arctic 2002/2003 winters, *J. Geophys. Res. Atmos.*, *110*, D24308, doi:10.1029/2005JD006463.

Funke, B., M. López-Puertas, H. Fischer, G. P. Stiller, T. von Clarmann, G. Wetzel, B. Carli, and C. Belotti (2007), Comment on "Origin of the January–April 2004 increase in stratospheric NO_2 observed in northern polar latitudes" by Jean-Baptiste Renard et al., *Geophys. Res. Lett.*, *34*, L07813, doi:10.1029/2006GL027518.

Funke, B., et al. (2011), Composition changes after the "Halloween" solar proton event: The high energy particle precipitation in the atmosphere (HEPPA) model versus MIPAS data intercomparison study, *Atmos. Chem. Phys.*, *11*(17), 9089–9139, doi:10.5194/acp-11-9089-2011.

Garcia, R. R., M. López-Puertas, B. Funke, D. R. Marsh, D. E. Kinnison, A. K. Smith, and F. González-Galindo (2014), On the distribution of CO_2 and CO in the mesosphere and lower thermosphere, *J. Geophys. Res. Atmos.*, *119*, 5700–5718, doi:10.1002/2013JD021208.

Geller, M. A., et al. (2013), A comparison between gravity wave momentum fluxes in observations and climate models, *J. Clim.*, *26*(17), 6383–6405, doi:10.1175/JCLI-D-12-00545.1.

Grygalashvyly, M., E. Becker, and G. R. Sonnemann (2011), Gravity wave mixing and effective diffusivity for minor chemical constituents in the mesosphere/lower thermosphere, *Space Sci. Rev.*, *168*(1–4), 333–362, doi:10.1007/s11214-011-9857-x.

Hines, C. O. (1997a), Doppler-spread parameterization of gravity-wave momentum deposition in the middle atmosphere. Part 1: Basic formulation, *J. Atmos. Sol. Terr. Phys.*, *59*(4), 371–386, doi:10.1016/S1364-6826(96)00079-X.

Hines, C. O. (1997b), Doppler-spread parameterization of gravity-wave momentum deposition in the middle atmosphere. Part 2: Broad and quasi monochromatic spectra, and implementation, *J. Atmos. Sol. Terr. Phys.*, *59*(4), 387–400, doi:10.1016/S1364-6826(96)00080-6.

Hoffmann, P., M. Rapp, W. Singer, and D. Keuer (2011), Trends of mesospheric gravity waves at northern middle latitudes during summer, *J. Geophys. Res.*, *116*, D00P08, doi:10.1029/2011JD015717.

Holt, L. A., C. E. Randall, E. D. Peck, D. R. Marsh, A. K. Smith, and V. L. Harvey (2013), The influence of major sudden stratospheric warming and elevated stratopause events on the effects of energetic particle precipitation in WACCM, *J. Geophys. Res. Atmos.*, *118*(20), 11,636–11,646, doi:10.1002/2013JD020294.

Huang, T., S. Walters, G. Brasseur, D. Hauglustaine, W. Wu, S. Chabrillat, T. Xuexi, C. Granier, A. Smith, and G. Kockarts (1998), Description of SOCRATES — A chemical dynamical radiative two-dimensional model, *NCAR Tech. Note NCAR/TN-440+EDD, NCAR*, Boulder, Colo.

Jackman, C. H., M. T. DeLand, G. J. Labow, E. L. Fleming, D. K. Weisenstein, M. K. W. Ko, M. Sinnhuber, and J. M. Russell (2005), Neutral atmospheric influences of the solar proton events in October–November 2003, *J. Geophys. Res.*, *110*, A09S27, doi:10.1029/2004JA010888.

Jones, M., J. M. Forbes, and M. E. Hagan (2014), Tidal-induced net transport effects on the oxygen distribution in the thermosphere, *Geophys. Res. Lett.*, *41*, 5272–5279, doi:10.1002/2014GL060698.

Kieser, J. (2011), *The Influence of Precipitating Solar and Magnetospheric Energetic Charged Particles on the Entire Atmosphere: Simulations With HAMMONIA*, Max-Planck-Inst. für Meteorologie, Germany.

Kinnison, D. E., et al. (2007), Sensitivity of chemical tracers to meteorological parameters in the MOZART-3 chemical transport model, *J. Geophys. Res. Atmos.*, *112*, D20302, doi:10.1029/2006JD007879.

Limpasuvan, V., J. H. Richter, Y. J. Orsolini, F. Stordal, and O.-K. Kvissel (2012), The roles of planetary and gravity waves during a major stratospheric sudden warming as characterized in WACCM, *J. Atmos. Sol. Terr. Phys.*, *78-79*, 84–98, doi:10.1016/j.jastp.2011.03.004.

Lin, S.-J., and R. B. Rood (1996), Multidimensional flux-form semi-Lagrangian transport schemes, *Mon. Weather Rev.*, *124*(9), 2046–2070, doi:10.1175/1520-0493(1996)124<2046:MFFSLT>2.0.CO;2.

Liu, A. Z. (2009), Estimate eddy diffusion coefficients from gravity wave vertical momentum and heat fluxes, *Geophys. Res. Lett.*, *36*, L08806, doi:10.1029/2009GL037495.

Manney, G. L., M. J. Schwartz, K. Krüger, M. L. Santee, S. Pawson, J. N. Lee, W. H. Daffer, R. A. Fuller, and N. J. Livesey (2009), Aura Microwave Limb Sounder observations of dynamics and transport during the record-breaking 2009 Arctic stratospheric major warming, *Geophys. Res. Lett.*, *36*, L12815, doi:10.1029/2009GL038586.

Peck, E. D., C. E. Randall, J. C. Green, J. V. Rodriguez, and C. J. Rodger (2015), POES MEPED differential flux retrievals and electron channel contamination correction, *J. Geophys. Res. Space Physics*, *120*, 4596–4612, doi:10.1002/2014JA020817.

Pedatella, N. M., et al. (2014), The neutral dynamics during the 2009 sudden stratosphere warming simulated by different whole atmosphere models, *J. Geophys. Res. Space Physics*, *119*, 1306–1324, doi:10.1002/2013JA019421.

Randall, C. E., V. L. Harvey, C. S. Singleton, P. F. Bernath, C. D. Boone, and J. U. Kozyra (2006), Enhanced NO_x in 2006 linked to strong upper stratospheric Arctic vortex, *Geophys. Res. Lett.*, *33*, L18811, doi:10.1029/2006GL027160.

Randall, C. E., V. L. Harvey, C. S. Singleton, S. M. Bailey, P. F. Bernath, M. Codrescu, H. Nakajima, and J. M. Russell (2007), Energetic particle precipitation effects on the Southern Hemisphere stratosphere in 1992–2005, *J. Geophys. Res.*, *112*, D08308, doi:10.1029/2006JD007696.

Randall, C. E., V. L. Harvey, D. E. Siskind, J. France, P. F. Bernath, C. D. Boone, and K. A. Walker (2009), NO_x descent in the Arctic middle atmosphere in early 2009, *Geophys. Res. Lett.*, *36*, L18811, doi:10.1029/2009GL039706.

Rodger, C. J., M. A. Clilverd, J. C. Green, and M. M. Lam (2010), Use of POES SEM-2 observations to examine radiation belt dynamics and energetic electron precipitation into the atmosphere, *J. Geophys. Res.*, *115*, A04202, doi:10.1029/2008JA014023.

Roeckner, E., R. Brokopf, M. Esch, M. Giorgetta, S. Hagemann, L. Kornblueh, E. Manzini, U. Schlese, and U. Schulzweida (2006), Sensitivity of simulated climate to horizontal and vertical resolution in the ECHAM5 atmosphere model, *J. Clim.*, *19*(16), 3771–3791, doi:10.1175/JCLI3824.1.

Rusch, D., J.-C. Gérard, S. Solomon, P. Crutzen, and G. Reid (1981), The effect of particle precipitation events on the neutral and ion chemistry of the middle atmosphere - I. Odd nitrogen, *Planet. Space Sci.*, *29*(7), 767–774, doi:10.1016/0032-0633(81)90048-9.

Sander, S. P., et al. (2006), *Chemical Kinetics and Photochemical Data for Use in Atmospheric Studies, Evaluation No. 15*, Jet Propul. Lab., Pasadena, Calif.

Schmidt, H., G. P. Brasseur, M. Charron, E. Manzini, M. A. Giorgetta, T. Diehl, V. I. Fomichev, D. Kinnison, D. Marsh, and S. Walters (2006), The HAMMONIA chemistry climate model: Sensitivity of the mesopause region to the 11-year solar cycle and CO_2 doubling, *J. Clim.*, *19*(16), 3903–3931, doi:10.1175/JCLI3829.1.

Schmidt, H., G. P. Brasseur, and M. A. Giorgetta (2010), Solar cycle signal in a general circulation and chemistry model with internally generated quasi-biennial oscillation, *J. Geophys. Res.*, *115*, D00I14, doi:10.1029/2009JD012542.

Semeniuk, K., J. C. McConnell, and C. H. Jackman (2005), Simulation of the October–November 2003 solar proton events in the CMAM GCM: Comparison with observations, *Geophys. Res. Lett.*, *32*, L15S02, doi:10.1029/2005GL022392.

Seppälä, A., and M. A. Clilverd (2014), Energetic particle forcing of the Northern Hemisphere winter stratosphere: Comparison to solar irradiance forcing, *Atmos. Sci.*, *2*, 25, doi:10.3389/fphy.2014.00025.

Sinnhuber, M., B. Funke, T. von Clarmann, M. López-Puertas, and G. P. Stiller (2014), Variability of NO_x in the polar middle atmosphere from October 2003 to March 2004: Vertical transport versus local production by energetic particles, *Atmos. Chem. Phys. Discuss.*, *14*(1), 1–29, doi:10.5194/acpd-14-1-2014.

Smith, A. K. (2012), Global dynamics of the MLT, *Surv. Geophys.*, *33*(6), 1177–1230, doi:10.1007/s10712-012-9196-9.

Smith, A. K., R. R. Garcia, D. R. Marsh, and J. H. Richter (2011), WACCM simulations of the mean circulation and trace species transport in the winter mesosphere, *J. Geophys. Res.*, *116*, D20115, doi:10.1029/2011JD016083.

Solomon, S., D. W. Rusch, J. C. Gérard, G. C. Reid, and P. J. Crutzen (1981), The effect of particle precipitation events on the neutral and ion chemistry of the middle atmosphere: II. Odd hydrogen, *Planet. Space Sci.*, *29*(8), 885–893, doi:10.1016/0032-0633(81)90078-7.

Wissing, J. M., and M.-B. Kallenrode (2009), Atmospheric Ionization Module Osnabrück (AIMOS): A 3-D model to determine atmospheric ionization by energetic charged particles from different populations, *J. Geophys. Res.*, *114*, A06104, doi:10.1029/2008JA013884.